Exploiting Measurement Subspaces for Wideband Electromagnetic Induction Processing

Charles Ethan Hayes, Waymond R. Scott, Jr., and James H. McClellan

School of Electrical and Computer Engineering
Georgia Institute of Technology
Atlanta, GA, USA 30332-0250

ABSTRACT

Recent work with Wideband Electromagnetic Induction (WEMI) sensors has shown that a low-rank model can be used to exploit the measurements. The low-rank model has led to a new filterless processing framework for frequency-domain WEMI sensors, where projection operators can be used in both the frequency and spatial dimensions of the data. Previous work has used a single subspace from the projected measurements to perform target detection, classification, and localization. This work investigates the eight remaining measurement subspaces created by the projection operators and how they can be exploited to extract more information for WEMI processing.

Keywords: Wideband Electromagnetic Induction, filterless, low-rank, pre-processing, projection, interference removal, adaptive filtering, noise estimation

1. INTRODUCTION

Recent work with Wideband Electromagnetic Induction (WEMI) sensors has shown that a low-rank model can be used to exploit the WEMI measurements. The low-rank model has led to a new filterless processing framework for frequency-domain WEMI sensors, where projection operators can be used in both the frequency and spatial dimensions of the data. The new projection operators create nine measurement subspaces. Previous work has focused on how to process a single subspace where the target signal exists isolated from interferers. This work will investigate the other eight subspaces created and how each subspace can be used to further exploit the measurements. The additional subspaces provide information for improved hardware debugging, accurate background noise estimation, void detection, and increased signal extraction from interferers. The relation between the physical model and the contents of each subspace is investigated, and measured field data is presented to validate the subspace separation. Implications on hardware debugging and potentials for improved WEMI processing will be discussed. A large amount of the target response is mixed with the soil response and is, thus, lost when only using the single signal subspace. A method is provided to isolate this signal content from the soil response so it can be used in further processing.

2. MEASUREMENT MATRIX MODEL

In order to delve into the new pre-processing framework,[1] it is useful to review the physical model of the WEMI data. A frequency-domain WEMI system takes a complex measurement, $\tilde{m}(\omega, p)$, at a specific operating frequency, ω, and at a specific location of the sensor, p. Each measurement taken by the sensor contains four primary sources: the response from a target, $\tilde{s}$, the magnetic response of the soil, $\tilde{g}$, the self response from the sensor, $\tilde{r}$, and a random noise term that can be approximated as a complex Gaussian random value, $\tilde{\epsilon} \sim \mathcal{CN}(0, 2\sigma_\epsilon^2)$. The sensor measurement is modeled as

$$\tilde{m}(\omega, p) = \tilde{s}(\omega, p) + \tilde{g}(\omega, p) + \tilde{r}(\omega, p) + \tilde{\epsilon}. \tag{1}$$

Recent work[1,2] has shown that the target response can be modeled as a low-rank matrix when multiple frequencies and positions are processed jointly. This leads to creating a measurement matrix for further processing

by grouping M frequencies, $\boldsymbol{\omega}$, along the rows of a matrix and N positions, $\boldsymbol{p}$, along the columns to create $\tilde{\mathbf{M}}(\boldsymbol{\omega}, \boldsymbol{p}) = [\tilde{m}(\boldsymbol{\omega}_i, \boldsymbol{p}_j)]_{i,j}$ where $\tilde{\mathbf{M}} \in \mathfrak{C}^{M \times N}$. The matrix model can then be written as

$$\tilde{\mathbf{M}}(\boldsymbol{\omega}, \boldsymbol{p}) = \tilde{\mathbf{S}}(\boldsymbol{\omega}, \boldsymbol{p}) + \tilde{\mathbf{G}}(\boldsymbol{\omega}, \boldsymbol{p}) + \tilde{\mathbf{R}}(\boldsymbol{\omega}, \boldsymbol{p}) + \tilde{\mathcal{E}} \tag{2}$$

where it is assumed that each noise term in $\tilde{\mathcal{E}}$ is an i.i.d. complex noise measurement. Finally, because the received signal only has a single complex component,[2] the measured data can be split into the real and imaginary components to be processed jointly across frequencies. This expansion can be written as

$$\mathbf{M}(\boldsymbol{\omega}, \boldsymbol{p}) = \begin{bmatrix} \Re\{\tilde{\mathbf{M}}(\boldsymbol{\omega}, \boldsymbol{p})\} \\ \Im\{\tilde{\mathbf{M}}(\boldsymbol{\omega}, \boldsymbol{p})\} \end{bmatrix} \tag{3}$$

where $\mathbf{M} \in \Re^{2M \times N}$ is the new real-valued measurement matrix. The model for the real-valued measurements becomes

$$\mathbf{M}(\boldsymbol{\omega}, \boldsymbol{p}) = \mathbf{S}(\boldsymbol{\omega}, \boldsymbol{p}) + \mathbf{G}(\boldsymbol{\omega}, \boldsymbol{p}) + \mathbf{R}(\boldsymbol{\omega}, \boldsymbol{p}) + \mathcal{E} \tag{4}$$

where each term has been separated as in (3).

As this work is focused on exploiting the new filterless pre-processing scheme[1] that uses projection matrices on $\mathbf{M}$, it is necessary to further investigate the matrix components. The target response has been discussed in previous work,[2] and the low-rank model for a target will be used for this work to model $\mathbf{S}$. The noise has been modeled as i.i.d. noise measurements, which means that each element of $\mathcal{E}$ is assumed to be drawn from i.i.d. $\mathcal{N}(0, \sigma_\epsilon^2)$ distributions. The remaining two components are discussed below and can be regarded as interference signals because they are always present in the measurements and interfere with the desired target response.

2.1 Self Response Matrix

The self response $\tilde{r}(\omega, p)$ is an artifact from the transmitter coil and receiver coils of the WEMI system coupling together. Given a specific operating frequency, this coupling is expected to be relatively constant over multiple positions because the sensor platform moves as a unit and should have a relatively steady response. This allows the self response to be modeled over multiple positions as $\tilde{\boldsymbol{r}}(\omega, \boldsymbol{p}) = \tilde{r}(\omega)\mathbf{1}^T$, where $\mathbf{1} \in \Re^{N \times 1}$ is a vector of 1's. Each operating frequency can have a different coupling response, and the phase of the coupling response is also unknown. Because of this, each operating frequency's real and imaginary part is assumed unknown and the self response matrix is modeled as

$$\mathbf{R}(\boldsymbol{\omega}, \boldsymbol{p}) = \boldsymbol{r}(\boldsymbol{\omega})\mathbf{1}^T \tag{5}$$

where $\boldsymbol{r} \in \Re^{2M \times 1}$ is an unknown vector of the system coupling responses.

It should be noted that the constant coupling response is an approximation. As long as the drift is small enough for the sensor and the window of position values, N, is short enough, then this approximation is expected to be true. However if either of these conditions is not met, then it may require the self response position model to be expanded into a more sophisticated model such as the linear model $\tilde{\boldsymbol{r}}(\omega, \boldsymbol{p}) = b + m\boldsymbol{p}$.

In a WEMI system, the self response is partially mitigated by the hardware design by nulling the coupling between the coils in the system. Even after the hardware nulling, the self response of the system is often multiple magnitudes greater than the average target response as will be evident in the results below. Because nulling is not sufficient, the remaining part of the self response must be mitigated using processing. Several types of filters have been investigated for mitigating the effects of the self response, and, generally, a single filter that is constrained to be zero mean has been used[3–5] although multiple filters constrained to be zero mean have been used.[6]

2.2 Soil Matrix

The soil response has been studied previously[7] where an empirical model for the soil response was found. The soil response is mostly contained in a two-dimensional subspace within the operating frequency dimension. This allows the soil response to be described as

$$\tilde{g}(\omega, p) = \begin{bmatrix} 1 & \log(\frac{\omega}{\omega_c}) + \frac{j\pi}{2} \end{bmatrix} \begin{bmatrix} \xi_1(p) \\ \xi_2(p) \end{bmatrix} \tag{6}$$

where $\xi_1(p)$ and $\xi_2(p)$ are the strengths of the soil response in these dimensions at a given position. These strengths will be dependent on the properties of the soil at each position as well as the geometry of the WEMI sensor. In order to be as general as possible, this work will model only the mean and variance of this soil strength function. This is equivalent to modeling the strength terms as Gaussian distributions such that $\xi_1(p) \sim \mathcal{N}(g_1, \sigma_g^2)$ and $\xi_2(p) \sim \mathcal{N}(g_2, \sigma_g^2)$. If the frequency model of the soil is expanded into a matrix and the real and imaginary parts are separated as in (3), then the soil matrix can be modeled as

$$\mathbf{G}(\boldsymbol{\omega}, \boldsymbol{p}) = \boldsymbol{\Psi}(\boldsymbol{\omega})\boldsymbol{\Xi}^T \tag{7}$$

where $\boldsymbol{\Psi} \in \Re^{2M \times 2}$ and $\boldsymbol{\Xi} \in \Re^{N \times 2}$.

2.3 Data Corroboration

In order to validate the measurement model, data[7] was processed to illustrate the model. The data at the beginning of the first lane was used to validate the measurement model. A matrix of data from the beginning of the lane was used because it will not have a target response and should only contain the other three terms: the self response, soil response, and random noise. The model for the self response and soil response predict that the data matrix should have a rank of three or less because the self response is rank one and the soil response is rank two. Because of the low-rank nature of the these interference responses, a singular value decomposition (SVD) can be used to determine that the data is accurately modeled with rank three or less. The remaining noise term is expected to make the data matrix full rank where the rest of the singular values are roughly equal. These results are shown in Fig. 1 along with the singular values of the data after the interference has been removed with projection operators.

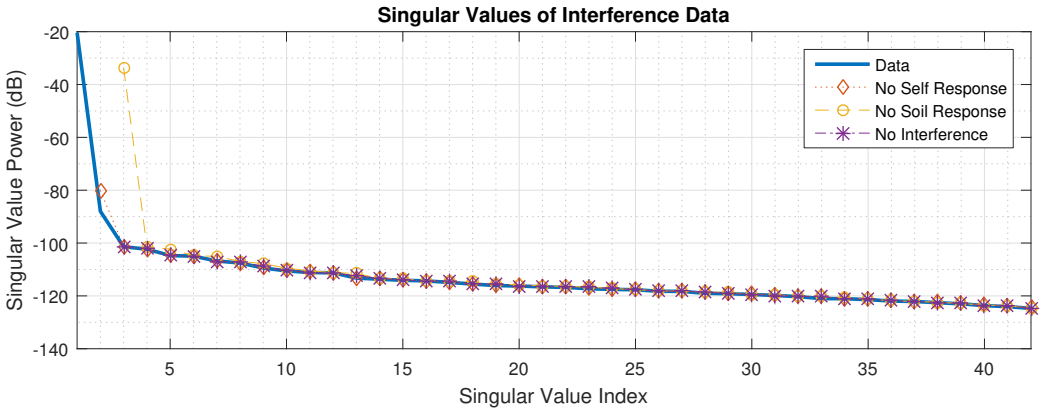

Figure 1: The singular values of a measured data matrix that does not contain any targets. The accuracy of the measurement model is shown by the singular values that remain after the soil and self response are removed.

The singular values of the data show that there is a single strong response in the raw data followed by another weaker response around -87 dB. The remaining singular values appear to be due to the noise floor. The self response is mostly mitigated when a constant term in the spatial domain is removed, this clearly lowers the first singular value. The second singular value increases slightly from this operation because the soil response that does not overlap with the constant spatial term is forced into this singular value. The soil response is mostly mitigated by projecting the data away from the soil model, the singular values are also shown when only the soil

response is removed. Although the soil response accounts for some of the interference, it is obvious that there is still a strong interferer remaining which corresponds to the self response according to the model. Finally, both the self and soil responses are removed, and the singular values align exactly with the original data's noise floor where the strongest singular values from the interference are removed. This suggests that the measurement model fits the measured data accurately. It is interesting to note that the two interference terms overlap significantly and only appear to have a total rank of two.

3. PROJECTIONS

3.1 Portioning out the measurement matrix

In order to best exploit the frequency-domain WEMI data, it is desirable to isolate the target response. Improved target isolation should translate into greater achievable processing gains. Previous work[1] has proposed using a filterless pre-processing scheme to isolate the target signal. This strategy uses two orthonormal projection matrices: $\mathbf{P_R}$ and $\mathbf{P_G}$. $\mathbf{P_R}$ is a projection matrix applied to the position dimension and is responsible for isolating the self response into a low-dimensional subspace, leaving a useful subspace where the target signal is isolated from the self response. For the ground response $\mathbf{P_G}$ performs the same function as $\mathbf{P_R}$ except on the operating frequency dimension, which means it creates a low-dimensional soil subspace as well as a subspace with the target isolated from the soil in the operating frequency dimension. These projection matrices are applied to the measurements $\mathbf{M}$ as shown in Figure 2 to create a decomposition of the signal into nine blocks. Previously, $\mathbf{M}_{\bar{\mathbf{G}}\mathbf{S}}^{\bar{\mathbf{R}}\mathbf{S}}$ was the only block used because the target signal has high SNR and is isolated from both the soil and self response.[1] This work will investigate each measurement block to develop a further understanding of how the data can best be exploited. In order to investigate the nine data blocks, it is necessary to first elaborate on the projection matrices used.

$$\mathbf{P_G M P_R}^H = \begin{array}{ccc} \mathbf{M}_{\bar{\mathbf{G}}\mathbf{S}}^{\mathbf{R}\mathbf{R}} & \mathbf{M}_{\bar{\mathbf{G}}\mathbf{S}}^{\bar{\mathbf{R}}\mathbf{S}} & \mathbf{M}_{\bar{\mathbf{G}}\mathbf{S}}^{\bar{\mathbf{R}}\mathcal{E}} \\ \mathbf{M}_{\bar{\mathbf{G}}\mathcal{E}}^{\mathbf{R}\mathbf{R}} & \mathbf{M}_{\bar{\mathbf{G}}\mathcal{E}}^{\bar{\mathbf{R}}\mathbf{S}} & \mathbf{M}_{\bar{\mathbf{G}}\mathcal{E}}^{\bar{\mathbf{R}}\mathcal{E}} \\ \mathbf{M}_{\mathbf{G}\mathbf{G}}^{\mathbf{R}\mathbf{R}} & \mathbf{M}_{\mathbf{G}\mathbf{G}}^{\bar{\mathbf{R}}\mathbf{S}} & \mathbf{M}_{\mathbf{G}\mathbf{G}}^{\bar{\mathbf{R}}\mathcal{E}} \end{array}$$

Projected away from soil subspace
Projected into target subspace
Mostly target response

Projected away from soil subspace
Projected away from target subspace
Mostly noise

Projected into soil subspace
Mostly soil response with some target

Low-Spatial frequencies
Mostly self response

Mid-Spatial frequencies
Mostly target response

High-Spatial frequencies
Mostly noise

(8)

Figure 2: Orthogonal projections for soil and self response applied to raw measurements $\mathbf{M}$.

3.2 Creating $\mathbf{P_G}$

The first projection matrix that will be investigated is $\mathbf{P_G}$. The creation of the projection matrix $\mathbf{P_G}$ is based on earlier work for computing the Discrete Spectrum of Relaxation Frequencies (DSRF).[8] Previous work took

advantage of the terms in $\mathbf{M}$ that are known to be dependent on the operating frequencies. Two terms, the soil and the target response, have known frequency dependencies. As described in (6), the soil has a two-dimensional model in the operating frequency domain. The target signal also has an operating frequency dependence that varies between targets, but the DSRF model[9] allows it to be represented by a sparse selection of the DSRF dictionary $\mathbf{A}$. The DSRF dictionary $\mathbf{A}$ contains templates for multiple possible relaxation frequencies $\boldsymbol{\zeta}$ that a target may have. Each element of $\mathbf{A}$ is defined as

$$\tilde{a}(\omega, \zeta) = \frac{j\omega/\zeta}{1 + j\omega/\zeta} \tag{9}$$

which serves as a mapping from a target's relaxation frequency to a WEMI system's measurement frequency. The dictionary $\mathbf{A}$ is created by selecting a set of possible discrete relaxation frequencies, $\boldsymbol{\zeta}$, and mapping them to the WEMI measurement frequencies, $\boldsymbol{\omega}$. This creates a complex-valued matrix that is separated as in (3) to create a real-valued matrix. Often $\boldsymbol{\zeta}$ is chosen as 100 equally logarithmically-spaced frequencies from just below the minimum operating frequency to just above the maximum operating frequency. Previously it was shown that by combining the dictionary $\mathbf{A}$ with the knowledge of the soil model, a set of projected operating frequency measurements could be created that were isolated from the soil.[8] This is accomplished through a two-step process. First, a projection matrix into the soil subspace is created in the standard manner as $\mathbf{P_{GG}} = \boldsymbol{\Psi}(\boldsymbol{\Psi}^T\boldsymbol{\Psi})^{-1}\boldsymbol{\Psi}^T$. This allows $\mathbf{A}$ to be defined as

$$\mathbf{A} = \mathbf{P_{GG}}\mathbf{A} + \mathbf{P}^{\perp}_{\mathbf{GG}}\mathbf{A} \tag{10}$$

where $\mathbf{P}^{\perp}_{\mathbf{GG}} = \mathbf{I} - \mathbf{P_{GG}}$ is the projection into the space orthogonal of the soil projection matrix. The second stage is to apply a singular value decomposition (SVD) to both terms in (10) which arrives at

$$\mathbf{A} = \mathbf{U}^{\mathbf{A}}_{\mathbf{G}}\boldsymbol{\Sigma}^{\mathbf{A}}_{\mathbf{G}}{\mathbf{V}^{\mathbf{A}}_{\mathbf{G}}}^T + \mathbf{U}^{\mathbf{A}}_{\bar{\mathbf{G}}}\boldsymbol{\Sigma}^{\mathbf{A}}_{\bar{\mathbf{G}}}{\mathbf{V}^{\mathbf{A}}_{\bar{\mathbf{G}}}}^T. \tag{11}$$

The singular values of the dictionary perpendicular to the soil, $\mathbf{P}^{\perp}_{\mathbf{GG}}\mathbf{A}$, can be used to estimate how much weaker the target signal will be in each of the projected frequency terms. A maximum target SNR requirement can be selected for the system which allows a singular value threshold, $\lambda_{\mathbf{G}\mathcal{E}}$, to be selected. If the terms in $\boldsymbol{\Sigma}^{\mathbf{A}}_{\bar{\mathbf{G}}}$ are normalized by the strongest singular value, then any term below $\lambda_{\mathbf{G}\mathcal{E}}$ can be ignored when reconstructing the data. The reconstructed signal will have a new "noise term" that will be roughly $\lambda_{\mathbf{G}\mathcal{E}}$ smaller than the target response. Using this threshold to separate the singular value terms of $\mathbf{P}^{\perp}_{\mathbf{GG}}\mathbf{A}$, the DSRF dictionary can be represented as

$$\mathbf{A} = \begin{bmatrix}\mathbf{U}^{\mathbf{A}}_{\bar{\mathbf{G}}\mathbf{S}} & \mathbf{U}^{\mathbf{A}}_{\bar{\mathbf{G}}\mathcal{E}} & \mathbf{U}^{\mathbf{A}}_{\mathbf{G}}\end{bmatrix}\begin{bmatrix}\boldsymbol{\Sigma}^{\mathbf{A}}_{\bar{\mathbf{G}}\mathbf{S}} & 0 & 0\\ 0 & \boldsymbol{\Sigma}^{\mathbf{A}}_{\bar{\mathbf{G}}\mathcal{E}} & 0\\ 0 & 0 & \boldsymbol{\Sigma}^{\mathbf{A}}_{\mathbf{G}}\end{bmatrix}\begin{bmatrix}{\mathbf{V}^{\mathbf{A}}_{\bar{\mathbf{G}}\mathbf{S}}}^T\\ {\mathbf{V}^{\mathbf{A}}_{\bar{\mathbf{G}}\mathcal{E}}}^T\\ {\mathbf{V}^{\mathbf{A}}_{\mathbf{G}}}^T\end{bmatrix} \tag{12}$$

where $\mathbf{U}^{\mathbf{A}}_{\bar{\mathbf{G}}}\boldsymbol{\Sigma}^{\mathbf{A}}_{\bar{\mathbf{G}}}{\mathbf{V}^{\mathbf{A}}_{\bar{\mathbf{G}}}}^T = \mathbf{U}^{\mathbf{A}}_{\bar{\mathbf{G}}\mathbf{S}}\boldsymbol{\Sigma}^{\mathbf{A}}_{\bar{\mathbf{G}}\mathbf{S}}{\mathbf{V}^{\mathbf{A}}_{\bar{\mathbf{G}}\mathbf{S}}}^T + \mathbf{U}^{\mathbf{A}}_{\bar{\mathbf{G}}\mathcal{E}}\boldsymbol{\Sigma}^{\mathbf{A}}_{\bar{\mathbf{G}}\mathcal{E}}{\mathbf{V}^{\mathbf{A}}_{\bar{\mathbf{G}}\mathcal{E}}}^T$ has been decomposed into a target response and a noise response and the addition of all three terms has been rewritten as a combination of three low-rank matrices. This decomposition looks like a SVD, but it is worth noting that this is not a direct SVD of $\mathbf{A}$ because ${\mathbf{V}^{\mathbf{A}}_{\mathbf{G}}}^T\mathbf{V}^{\mathbf{A}}_{\bar{\mathbf{G}}\mathbf{S}} \neq 0$ and ${\mathbf{V}^{\mathbf{A}}_{\mathbf{G}}}^T\mathbf{V}^{\mathbf{A}}_{\bar{\mathbf{G}}\mathcal{E}} \neq 0$.

The decomposition of $\mathbf{A}$ in (12) is useful because the desired orthonormal matrix $\mathbf{P_G}$ can now be defined as

$$\mathbf{P_G} = \begin{bmatrix}\mathbf{P}_{\bar{\mathbf{G}}\mathbf{S}}\\ \mathbf{P}_{\bar{\mathbf{G}}\mathcal{E}}\\ \mathbf{P_{GG}}\end{bmatrix} = \begin{bmatrix}\mathbf{U}^{\mathbf{A}}_{\bar{\mathbf{G}}\mathbf{S}} & \mathbf{U}^{\mathbf{A}}_{\bar{\mathbf{G}}\mathcal{E}} & \mathbf{U}^{\mathbf{A}}_{\mathbf{G}}\end{bmatrix}^T. \tag{13}$$

For notational clarification, even though $\mathbf{P_{GG}} = \mathbf{U}^{\mathbf{A}}_{\mathbf{G}}$ is not guaranteed, they are guaranteed to span the same subspace and be orthonormal, so from a projection operator stance they are equivalent.

The frequency projection matrix, $\mathbf{P_G}$, can be calculated off-line prior to the measurements as long as the soil subspace is known. The only necessary tuning parameter is choosing $\lambda_{\mathbf{G}\mathcal{E}}$. Fig 3 shows the singular values from realistic DSRF dictionaries for determining $\lambda_{\mathbf{G}\mathcal{E}}$. These plots assume that a WEMI system was designed to span the frequency range from 330 Hz to 90 kHz. The system measures 7, 14, 21, or 28 equally log-spaced

frequencies in this range respectively. The DSRF dictionary is then created by using 100 equally log-spaced relaxation frequencies from 44 Hz to 667 kHz (roughly 0.87 decades beyond the measured frequencies). These design parameters are used for (9)-(12), and the singular values are shown in Fig. 3. It is also of interest to know how much of the target response is expected to be lost to the soil subspace. In order to illustrate the target loss, the singular values of the original dictionary before projecting away from the soil subspace are also shown in Fig. 3.

It is interesting to note that the number of measurement frequencies has little impact on the shape of the singular values. However, more measurement frequencies make a larger range of singular values. This enables a lower threshold $\lambda_{\mathbf{G}\mathcal{E}}$ to be chosen while still leaving a reasonable size noise subspace for future operations. This work uses data from a Georgia Tech frequency-domain WEMI system that uses the same operating characteristics with 21 measurement frequencies. This work selected 100 dB as the cutoff threshold $\lambda_{\mathbf{G}\mathcal{E}}$, which translates into having 21 projected frequency measurements in the signal subspace, 19 measurements in the noise subspace, and 2 measurements in the soil subspace. This threshold was also chosen because it is expected that further WEMI processing should be able to exploit targets in 100 dB SNR or lower, so the information lost due to this threshold should be insignificant.

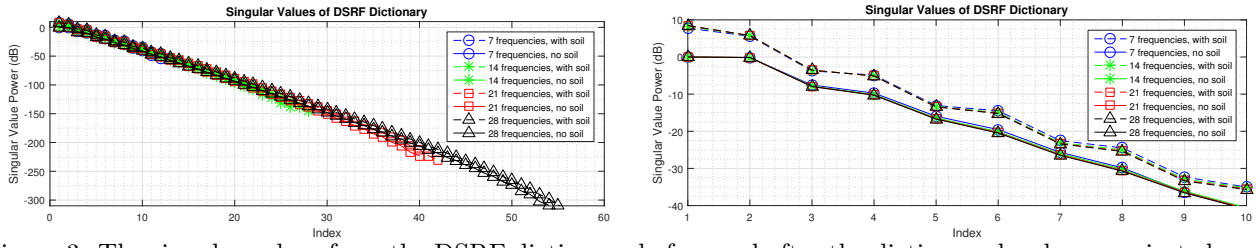

Figure 3: The singular values from the DSRF dictionary before and after the dictionary has been projected away from the soil subspace.

As can be seen in Fig. 3, the largest singular value of $\mathbf{P}^{\perp}_{\mathbf{GG}}\mathbf{A}$ is 8.5 dB smaller than the largest singular value of the original dictionary $\mathbf{A}$. This means that the largest response of a target in measured data will decrease by roughly 8.5 dB when projecting the target away from the soil response. This is a significant drop that motivates a later discussion on how this data can be potentially recovered. It should be noted however that this is only the energy drop from the strongest component. Fig 4 shows the ratio of the total power in the DSRF dictionary after it has been isolated from the soil to the total power of the original dictionary. Mathematically this was calculated as $\delta_g = \|\mathbf{P}^{\perp}_{\mathbf{GG}}\mathbf{A}\|_F^2 / \|\mathbf{A}\|_F^2$.

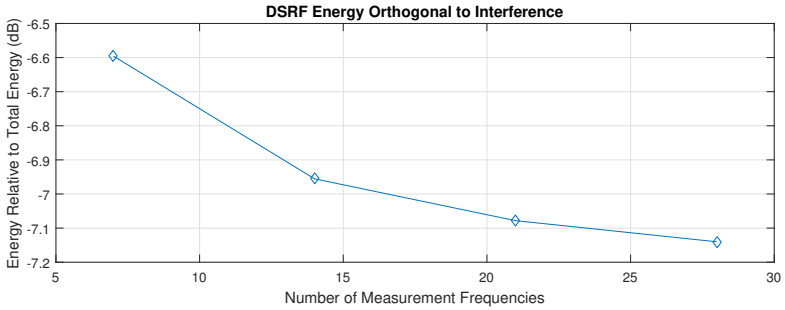

Figure 4: The ratio of the DSRF dictionary after being isolated from the soil compared to the total power.

3.3 Creating $\mathbf{P_R}$

The spatial domain projection matrix, $\mathbf{P_R}$, must also be created. The current $\mathbf{P_R}$ matrix is inspired by previous frequency-domain WEMI filters. An elegant and highly effective non-adaptive filter for frequency-domain WEMI sensors with a quadrupole receiver is the sine filter. The sine filter is a rough approximation of the target response as it passes under the receiver. Fig. 5 shows how the sine filter is designed to mimic the spatial dimension of a

target response as it passes under the positive and then negatively polarized receiver. The traditional sine filter is usually tuned to the spatial wavelength of the system.

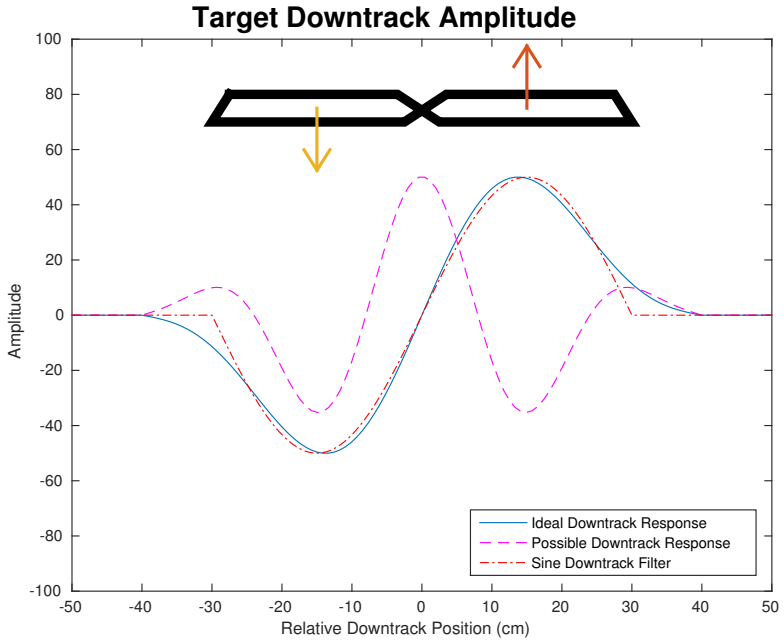

Figure 5: An illustration of how the sine filter is an approximate matched filter to a target response when using a quadrupole receiver.

The most direct extension of the sine filter into a projection matrix is to use a Discrete Fourier Transform (DFT). This is intuitively the same as using a filter bank of multiple sine filters. The DFT is effective, but previous work has migrated to using the Discrete Cosine Transform (DCT) matrix[1,5] for two reasons. The first reason is that the DCT is more robust when the target is on the edge of the spatial window. The second reason is that the DFT would convert the real-valued matrix back into complex-values, but the DCT projects the measured data into a new real-valued matrix. Keeping the data as real-valued is beneficial when it comes to quickly and easily operating on the data in future stages, such as the DSRF recovery problem.

In order to show the difference between the DCT and DFT as a projection matrix, Fig. 6 illustrates both projections being used on a simulated target. Fig. 6a is a target of rank two that is centered directly under the sensor. The measurements are projected into the DFT (Fig. 6c) and DCT (Fig. 6d) domains respectively. The target's spatial response is then reconstructed by only using the terms orthogonal to the DC term and with a spatial wavelength larger than 5 cm. The reconstructed spatial response is plotted again in Fig. 6a to show that it is an accurate representation of the data. The same process was performed on the same simulated target when it was shifted to the edge of the measurement matrix. Fig. 6b shows that the reconstructed DFT data no longer accurately represents the signal because the DFT forces the samples on the edges to converge so the signal is continuous when circularly shifted in the window. The DCT projection is designed so that it does not enforce this edge artifact and thus can reconstruct the measured data. A few observations can be taken from Fig. 6d and 6c. First, the target's spatial response is mostly contained in terms with a wavelength longer than 5 cm. Second, the DCT contains less target response in the shorter wavelengths than the DFT. Finally, both the DCT and DFT greatly increase the target's power in the short wavelengths when the target is on the edge of the measurement matrix.

Both the DFT and DCT satisfy the constraints needed for $\mathbf{P_R}$. Both projections have a subspace that holds the constant (DC) component, and all other elements are orthogonal to the constant component (zero-mean). The longer wavelengths (lower spatial frequencies) can also be used to isolate the drift component of the self response if desired. It is also useful to point out that the target response should lie within a subset of the possible wavelengths (spatial frequencies) due to the physical design of the quadrupole receiver. Because of

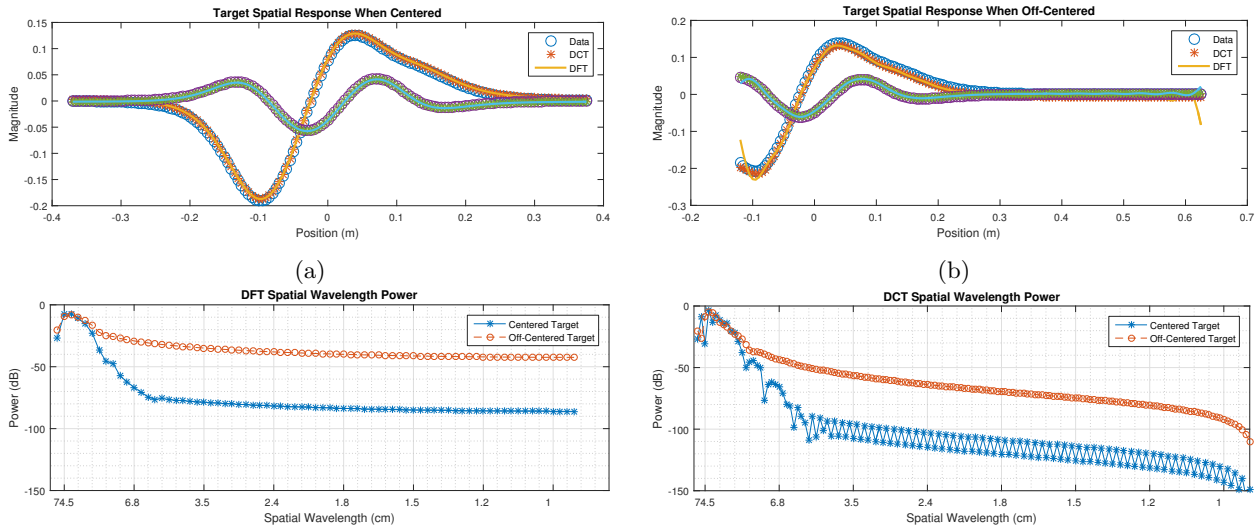

Figure 6: These plots show how well the DFT and DCT matrices can be used to isolate the spatial dimension of a target response. A target's spatial response was simulated and then reconstructed from a small subspace of the DFT and DCT matrices in (a) and (b). The power from the simulated target in the projected DFT and DCT domain are shown in (c) and (d) respectively.

this, any extremely short wavelength patterns (high spatial frequencies) can be assumed to not have any target response and thus only contain the noise term. This allows the self response projection matrix to be defined as

$$\mathbf{P_R} = \begin{bmatrix} \mathbf{P_{RR}} \\ \mathbf{P_{\bar{R}S}} \\ \mathbf{P_{\bar{R}\mathcal{E}}} \end{bmatrix} = \begin{bmatrix} \boldsymbol{\mathcal{D}}_L \\ \boldsymbol{\mathcal{D}}_M \\ \boldsymbol{\mathcal{D}}_S \end{bmatrix} = \boldsymbol{\mathcal{D}} \tag{14}$$

where $\boldsymbol{\mathcal{D}}_L$ contains the long spatial wavelengths that contain the self response, $\boldsymbol{\mathcal{D}}_M$ contain the expected spatial wavelengths for targets, and $\boldsymbol{\mathcal{D}}_S$ are the short spatial wavelengths that are expected to be noise. The wavelengths (spatial frequencies) to separate these subspaces are selected based on the receiver design.

4. MEASUREMENT MATRIX BLOCKS

With the detailed description of the pre-processing stages for the frequency-domain WEMI framework provided in Section 3.1, it is possible to investigate each of the sub-matrix data blocks shown in Fig. 2. Each data block is inspected below to create a mathematical formulation for what data is expected to be present. The mathematical model is paired with results from data obtained using the Georgia Tech frequency-domain WEMI system.[7] The data has been processed by creating data matrices that span roughly 75 cm. This creates a data matrix that is roughly the size $\mathbf{M} \in \Re^{42\times 175}$, where the number of spatial samples can vary slightly for each lane. The data matrix is pre-processed using $\lambda_{\mathbf{G}\mathcal{E}} = 100$dB and a minimum spatial wavelength of 5 cm. Each data block is shown for all 26 lanes collected with the sensor. The locations of metallic targets have been labeled with a filled circle and non-metallic targets are labeled with an empty diamond. In a few areas of the collected data, the target response was strong enough to significantly increase the sensor voltage. These strong targets potentially violate the assumptions of the model because they can overwhelm the sensor and cause model inaccuracies. Because these strong targets potentially violate the model, they have been circled in red as a warning that the results are potentially misleading. A discussion of how each data block can be used to improve processing is also included with the results.

4.1 Investigating $\mathbf{M}^{\mathbf{RR}}_{\bar{\mathbf{G}}\mathbf{S}}$

The data block $\mathbf{M}^{\mathbf{RR}}_{\bar{\mathbf{G}}\mathbf{S}}$ is designed to contain the overlap of the self response and the target response that is orthogonal from the ground. This is expressed mathematically as

$$\mathbf{P}_{\bar{\mathbf{G}}\mathbf{S}}\mathbf{M}\mathbf{P}^T_{\mathbf{RR}} = \cancel{\mathbf{P}_{\bar{\mathbf{G}}\mathbf{S}}\mathbf{S}\mathbf{P}^T_{\mathbf{RR}}}^{\epsilon} + \cancel{\mathbf{P}_{\bar{\mathbf{G}}\mathbf{S}}\mathbf{G}\mathbf{P}^T_{\mathbf{RR}}}^{0} + \mathbf{P}_{\bar{\mathbf{G}}\mathbf{S}}\mathbf{R}\mathbf{P}^T_{\mathbf{RR}} + \mathbf{P}_{\bar{\mathbf{G}}\mathbf{S}}\mathcal{E}\mathbf{P}^T_{\mathbf{RR}} \tag{15}$$

where it is noted that both the target response and soil response are expected to be negligible in this data block. The soil response should be completely removed because $\mathbf{P}_{\bar{\mathbf{G}}\mathbf{S}}$ was designed such that $\mathbf{P}_{\bar{\mathbf{G}}\mathbf{S}}\mathbf{G} \rightarrow \mathbf{0}$. The target response is expected to be some small value, ϵ, because of the design of the WEMI system. By using a quadrupole receiver, the target should change signs while passing below the receiver and have a zero-mean effect on the received measurements. Ideally, this indicates that $\mathbf{S}\mathbf{P}^T_{\mathbf{RR}} \rightarrow \epsilon$; however, the target response will leak into $\mathbf{M}^{\mathbf{RR}}_{\bar{\mathbf{G}}\mathbf{S}}$ when a) the sensor is tilted which skews the response making it no longer zero mean, b) the target is on the edge of the data matrix, $\mathbf{M}$, so it only contains part of the target response which is not zero mean, and c) the target has a tensor component that does not create a zero mean response. Other EMI sensors may not have a zero-mean response in normal operation and will always leak into $\mathbf{M}^{\mathbf{RR}}_{\bar{\mathbf{G}}\mathbf{S}}$.

Because the self response is expected to be the dominating term, this block is a useful metric in estimating how strong the coupling is between the transmitter and receiver. This can be used as a metric to test the design of the platform or for any other purpose where the self response is needed. When creating this block from the measured data, it was $\mathbf{M}^{\mathbf{RR}}_{\bar{\mathbf{G}}\mathbf{S}} \in \Re^{21\times 1}$. Fig. 7 shows this data block's average power per sample across all of the measured lanes. As can be seen, the metric remains constant around an average power of -50dB across nearly all of the measurements. Only a few stronger targets distort this metric, mainly when they are on the edge of the data matrix which causes an increase in target leakage from $\mathbf{P}_{\mathbf{G}}$.

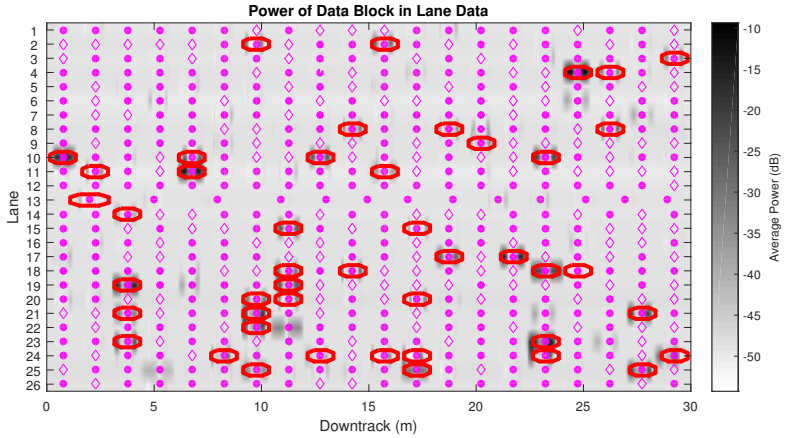

Figure 7: Average power of the $\mathbf{M}^{\mathbf{RR}}_{\bar{\mathbf{G}}\mathbf{S}}$ data block from measured WEMI data. This data block has low spatial frequencies and is orthogonal from the soil subspace while aligning with the target's DSRF. This data is expected to be dominated by the self response.

4.2 Investigating $\mathbf{M}^{\bar{\mathbf{R}}\mathbf{S}}_{\bar{\mathbf{G}}\mathbf{S}}$

The data block $\mathbf{M}^{\bar{\mathbf{R}}\mathbf{S}}_{\bar{\mathbf{G}}\mathbf{S}}$ is designed to contain the target response when it is orthogonal to both the ground and self response. This is expressed mathematically as

$$\mathbf{P}_{\bar{\mathbf{G}}\mathbf{S}}\mathbf{M}\mathbf{P}^T_{\bar{\mathbf{R}}\mathbf{S}} = \mathbf{P}_{\bar{\mathbf{G}}\mathbf{S}}\mathbf{S}\mathbf{P}^T_{\bar{\mathbf{R}}\mathbf{S}} + \cancel{\mathbf{P}_{\bar{\mathbf{G}}\mathbf{S}}\mathbf{G}\mathbf{P}^T_{\bar{\mathbf{R}}\mathbf{S}}}^{0} + \cancel{\mathbf{P}_{\bar{\mathbf{G}}\mathbf{S}}\mathbf{R}\mathbf{P}^T_{\bar{\mathbf{R}}\mathbf{S}}}^{0} + \mathbf{P}_{\bar{\mathbf{G}}\mathbf{S}}\mathcal{E}\mathbf{P}^T_{\bar{\mathbf{R}}\mathbf{S}} \tag{16}$$

where it is noted that both the self response and soil response are expected to be negligible in this data block. The soil response should be completely removed again because of the design of $\mathbf{P}_{\bar{\mathbf{G}}\mathbf{S}}$. The self response should also be completely removed because the design of $\mathbf{P}_{\bar{\mathbf{R}}\mathbf{S}}$ causes $\mathbf{R}\mathbf{P}^T_{\bar{\mathbf{R}}\mathbf{S}} \rightarrow 0$. This leaves only the target information

and noise in $\mathbf{M}^{\bar{\mathbf{R}}\mathbf{S}}_{\bar{\mathbf{G}}\mathbf{S}}$. It is useful to define this projected data block as $\mathbf{M_S} = \mathbf{P}_{\bar{\mathbf{G}}\mathbf{S}}\mathbf{M}\mathbf{P}^T_{\bar{\mathbf{R}}\mathbf{S}}$, the target response in this data block as $\mathbf{S_S} = \mathbf{P}_{\bar{\mathbf{G}}\mathbf{S}}\mathbf{S}\mathbf{P}^T_{\mathbf{RR}}$, and the noise matrix in $\mathbf{M}^{\bar{\mathbf{R}}\mathbf{S}}_{\bar{\mathbf{G}}\mathbf{S}}$ as $\mathcal{E}_\mathbf{S} = \mathbf{P}_{\bar{\mathbf{G}}\mathbf{S}}\mathcal{E}\mathbf{P}^T_{\bar{\mathbf{R}}\mathbf{S}}$ because they are of primary interest for future processing.

The average power of $\mathbf{M_S}$ is shown in Fig. 8, were it had a size of roughly $\mathbf{M_S} \in \Re^{21\times 29}$. The targets in the measured data correspond to an increase in average power as the model predicts. Also, it can be noted that the noise floor of the WEMI sensor has been reduced to an average power of -130dB.

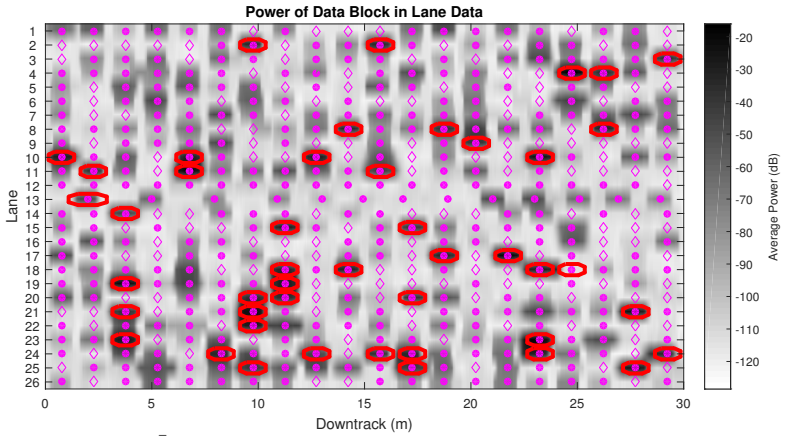

Figure 8: Average power of the $\mathbf{M}^{\bar{\mathbf{R}}\mathbf{S}}_{\bar{\mathbf{G}}\mathbf{S}}$ data block from measured WEMI data. This data block has the middle spatial frequencies and is orthogonal from the soil subspace while aligning with the target's DSRF. This data is expected to be dominated by the target response.

It is insightful to elaborate on the effect of the projection matrices on $\mathcal{E}$ at this point to describe the resulting signal-to-noise ratio (SNR) of the data block $\mathbf{M_S}$. Let $\mathbf{p}$ be any vector in a projection matrix. For this example, assume $\mathbf{p} \in \Re^{2M\times 1}$ is a row-vector from $\mathbf{P_G}$ that has been rotated into a column-vector. Given a vector of random i.i.d. Gaussian noise samples, $\boldsymbol{\epsilon} \in \Re^{2M\times 1}$, where each sample is drawn from the distribution $\mathcal{N}(0, \sigma^2_\epsilon)$, it can be easily shown that $\mathbf{p}^T\boldsymbol{\epsilon} \sim \mathcal{N}(0, \sigma^2_\epsilon)$ as long as $\|\mathbf{p}\|_2 = 1$. It can also be easily shown that as long as two projection vectors, $\mathbf{p}_i$ and $\mathbf{p}_j$, are orthogonal ($\mathbf{p}_i^T\mathbf{p}_j = 0$), then the new sample created from each projection vector will be independent ($\mathbf{p}_i^T\boldsymbol{\epsilon}$ and $\mathbf{p}_j^T\boldsymbol{\epsilon}$ are independent). Both of these constraints are true about all of the vectors within a projection matrix. This means that multiplying a noise vector by a projection matrix, $\mathbf{P}_{\bar{\mathbf{G}}\mathbf{S}}\boldsymbol{\epsilon}$, produces a new noise vector where each element is again i.i.d. $\mathcal{N}(0, \sigma^2_\epsilon)$. When the projection operator is applied to a matrix of i.i.d. samples it will create a new matrix of i.i.d. samples, $\mathbf{P}_{\bar{\mathbf{G}}\mathbf{S}}\mathcal{E} \in \Re^{O\times N}$. This procedure is repeated for the projection matrix on the other side to create a new noise matrix $\mathcal{E}_\mathbf{S} \in \Re^{O\times P}$ where each element is i.i.d. $\mathcal{N}(0, \sigma^2_\epsilon)$.

In order to discuss SNR, it is necessary to define the power metric. The power of a matrix will be defined as the squared Frobenius norm (the sum of each element squared). The average power of a matrix will be defined as the power divided by the number of elements in the matrix. Under these definitions, it is straight forward to calculate the expected power of the two noise matrices as $E\left[\|\mathcal{E}\|^2_F\right] = 2MN\sigma^2_\epsilon$ and $E\left[\|\mathcal{E}_\mathbf{S}\|^2_F\right] = OP\sigma^2_\epsilon$. This shows that the projections have reduced the expected noise power by a factor of $\frac{OP}{2MN}$ in $\mathcal{E}_\mathbf{S}$. Unlike the expected noise power, the signal power should be roughly unchanged except for the signal power that was projected into the soil subspace. This means that the signal power should be $\|\mathbf{S_S}\|^2_F \approx \delta_g\|\mathbf{S}\|^2_F$. By combining these observations, it is possible to define the SNR change from only the signal and noise terms through the projection operators as

$$E\left[\frac{\|\mathbf{S_S}\|^2_F}{\|\mathcal{E}_\mathbf{S}\|^2_F}\right] = \delta_g\frac{2MN}{OP}E\left[\frac{\|\mathbf{S}\|^2_F}{\|\mathcal{E}\|^2_F}\right] \tag{17}$$

where inserting the dimensions of the data produce $\frac{2MN}{OP} = \frac{42\cdot 175}{21\cdot 29} \approx 12$. This shows that the data block $\mathbf{M_S}$ can potentially have a SNR boost over the raw measurements $\mathbf{M}$ while also being isolated from interference signals.*

*It is also possible to perform these calculations on the average power, where it is seen that the expected average power for the noise remains unchanged at σ^2_ϵ, but the target average power increases by the amount in (17).

The data block $\mathbf{M_S}$ can be processed for further SNR improvement. Previous work has shown that the target response matrix $\mathbf{S}$ is low-rank, where it has a maximum rank of three for a dipole target.[2] The target's low-rank nature will also be true in $\mathbf{S_S}$ as the projections cannot increase the rank of the matrix. The target's low-rank can be exploited by taking a singular value decomposition (SVD) of the data block[1]

$$\mathbf{M_S} = \mathbf{U}_{\mathbf{M_S}} \mathbf{\Sigma}_{\mathbf{M_S}} {\mathbf{V}_{\mathbf{M_S}}}^T. \tag{18}$$

The target response will be contained in three singular values or less.[†] Ideal i.i.d. Gaussian noise will spread out evenly through all of the singular values. As long as the singular values of the target are larger than the noise, then they will be contained in the largest three singular values of $\mathbf{\Sigma}_{\mathbf{M_S}}$. This allows $\mathbf{M_S}$ to be further separated into two sub-blocks

$$\mathbf{M_S} = \begin{bmatrix} \mathbf{U}_{\mathbf{S}}^{\mathbf{M_S}} & \mathbf{U}_{\mathcal{E}}^{\mathbf{M_S}} \end{bmatrix} \begin{bmatrix} \mathbf{\Sigma}_{\mathbf{S}}^{\mathbf{M_S}} & 0 \\ 0 & \mathbf{\Sigma}_{\mathcal{E}}^{\mathbf{M_S}} \end{bmatrix} \begin{bmatrix} {\mathbf{V}_{\mathbf{S}}^{\mathbf{M_S}}}^T \\ {\mathbf{V}_{\mathcal{E}}^{\mathbf{M_S}}}^T \end{bmatrix} = \mathbf{U}_{\mathbf{S}}^{\mathbf{M_S}} \mathbf{\Sigma}_{\mathbf{S}}^{\mathbf{M_S}} {\mathbf{V}_{\mathbf{S}}^{\mathbf{M_S}}}^T + \mathbf{U}_{\mathcal{E}}^{\mathbf{M_S}} \mathbf{\Sigma}_{\mathcal{E}}^{\mathbf{M_S}} {\mathbf{V}_{\mathcal{E}}^{\mathbf{M_S}}}^T \tag{19}$$

by isolating the contents of the three largest singular values from the rest of the singular values in $\mathbf{M_S}$.

The low-rank target signal isolation was performed on the WEMI lane data. The only change was that the strongest six singular values were used for the target just in case distortion effects from the sensor caused a slightly larger rank than the model predicts. Fig. 9 shows the average power of the increased SNR signal within $\mathbf{\Sigma}_{\mathbf{S}}^{\mathbf{M_S}}$. Notice that the target response is minimally impacted by the operation. It should be noted that when a target is not present, the noise is only slightly decreased by the SVD because the strongest noise still remains. When a target is present, the above SNR discussion should hold true. Fig. 10 shows the average power of the noise removed from $\mathbf{M_S}$ in the singular values of $\mathbf{\Sigma}_{\mathcal{E}}^{\mathbf{M_S}}$. Notice that the remaining noise power is minimally correlated to when a target is present. Also, it is relatively constant at a low noise floor of roughly -130dB.

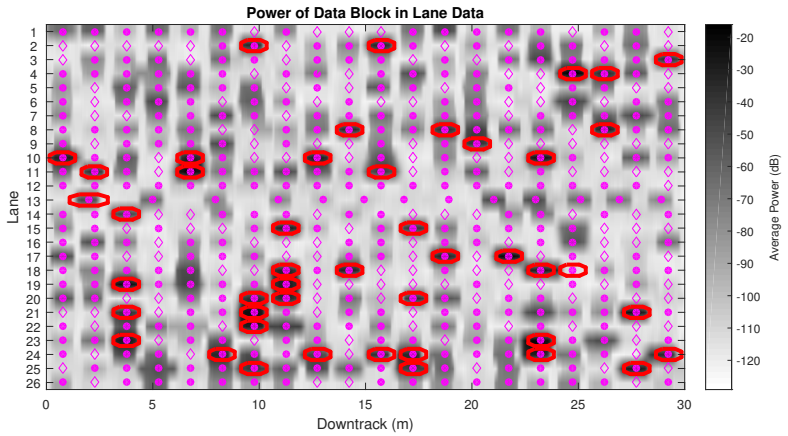

Figure 9: Average power of the $\mathbf{\Sigma}_{\mathbf{S}}^{\mathbf{M_S}}$ data block from measured WEMI data. This data block contains the low-rank approximation of $\mathbf{M}_{\bar{\mathbf{G}}\mathbf{S}}^{\bar{\mathbf{R}}\mathbf{S}}$ and is expected to further isolate the target response.

This process of further isolating the signal within $\mathbf{M_S}$ will further increase the SNR as long as the signal was originally strong enough for the SVD operation to isolate it into the largest singular vectors. The SNR increase can be calculated by exploiting the relationship between the Frobenius norm and singular values. By definition, the squared Frobenius norm is equivalent to the sum of the squared singular values of the matrix. This means that the expected power of the noise under an i.i.d. Gaussian assumption for the data block can also be described as

$$E\left[\|\mathcal{E}_{\mathbf{S}}\|_F^2\right] = OP\sigma_\epsilon^2 = \min\{O, P\} \cdot \lambda_{\mathcal{E}}^{\mathbf{M_S}} \tag{20}$$

where $\lambda_{\mathcal{E}}^{\mathbf{M_S}}\mathbf{I}$ are the singular values of $\mathcal{E}_{\mathbf{S}}$. When the sub-blocks of $\mathbf{M_S}$ are created, only three singular values remain. This means that the expected noise power becomes $(3\sigma_\epsilon^2) \cdot \max\{O, P\}$. Because the target response is

[†]Assumes the target is small enough to be treated as a dipole target.

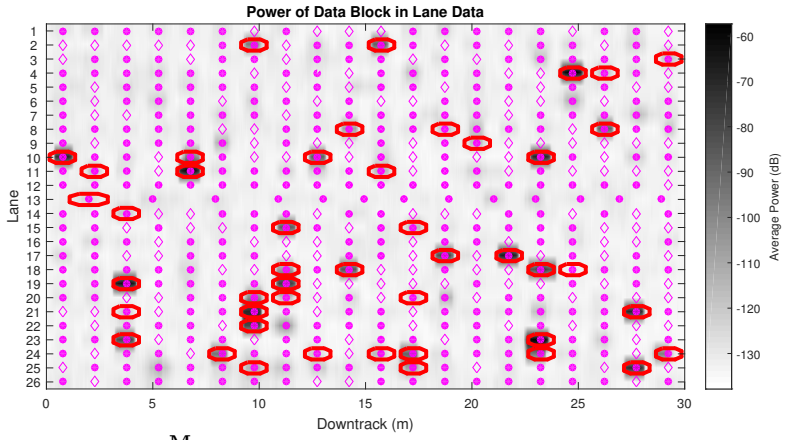

Figure 10: Average power of the $\mathbf{\Sigma}_{\mathcal{E}}^{\mathbf{M_S}}$ data block from measured WEMI data. This data block contains the remaining power of $\mathbf{M}_{\bar{\mathbf{G}}\mathbf{S}}^{\bar{\mathbf{R}}\mathbf{S}}$ after the low-rank approximation and is expected to contain only noise.

fully contained in the low-rank approximation, the final SNR becomes

$$\text{SNR}\left(\mathbf{U}_{\mathbf{S}}^{\mathbf{M_S}}\mathbf{\Sigma}_{\mathbf{S}}^{\mathbf{M_S}}\mathbf{V}_{\mathbf{S}}^{\mathbf{M_S}\,T}\right) = \frac{\min\{O,P\}}{3}\delta_g\frac{2MN}{OP}E\left[\frac{\|\mathbf{S}\|_F^2}{\|\mathcal{E}\|_F^2}\right] = \delta_g\frac{2MN}{3\cdot\max\{O,P\}}E\left[\frac{\|\mathbf{S}\|_F^2}{\|\mathcal{E}\|_F^2}\right] \tag{21}$$

where the dimensions for this data collection can be inserted to arrive at $\frac{2MN}{3\cdot\max\{O,P\}} = \frac{42\cdot175}{3\cdot29} \approx 84.5$.

4.3 Investigating $\mathbf{M}_{\bar{\mathbf{G}}\mathbf{S}}^{\bar{\mathbf{R}}\mathcal{E}}$

The data block $\mathbf{M}_{\bar{\mathbf{G}}\mathbf{S}}^{\bar{\mathbf{R}}\mathcal{E}}$ is designed to contain short spatial wavelength (high frequency) noise terms found in the spatial dimension that overlap with the target response orthogonal from the ground. This is expressed mathematically as $\mathbf{M}_{\bar{\mathbf{G}}\mathbf{S}}^{\bar{\mathbf{R}}\mathcal{E}}$

$$\mathbf{P}_{\bar{\mathbf{G}}\mathbf{S}}\mathbf{M}\mathbf{P}_{\bar{\mathbf{R}}\mathcal{E}}^T = \cancelto{\epsilon}{\mathbf{P}_{\bar{\mathbf{G}}\mathbf{S}}\mathbf{S}\mathbf{P}_{\bar{\mathbf{R}}\mathcal{E}}^T} + \cancelto{0}{\mathbf{P}_{\bar{\mathbf{G}}\mathbf{S}}\mathbf{G}\mathbf{P}_{\bar{\mathbf{R}}\mathcal{E}}^T} + \cancelto{0}{\mathbf{P}_{\bar{\mathbf{G}}\mathbf{S}}\mathbf{R}\mathbf{P}_{\bar{\mathbf{R}}\mathcal{E}}^T} + \mathbf{P}_{\bar{\mathbf{G}}\mathbf{S}}\mathcal{E}\mathbf{P}_{\bar{\mathbf{R}}\mathcal{E}}^T \tag{22}$$

where it is noted that all terms except the noise matrix are expected to be negligible in this data block. The soil response should be completely removed because $\mathbf{P}_{\bar{\mathbf{G}}\mathbf{S}}$ was designed such that $\mathbf{P}_{\bar{\mathbf{G}}\mathbf{S}}\mathbf{G} \to \mathbf{0}$. The target response is expected to be some small value, ϵ, because of the design of the WEMI system. By using a quadrupole receiver, the target should remain the same sign for shorter spatial wavelengths because the transmitter-receiver polarity will remain constant. Because of this, any sign variation in the response on this short of a spatial span is unlikely to be derived from that target. This means that $\mathbf{S}\mathbf{P}_{\bar{\mathbf{R}}\mathcal{E}}^T \to \epsilon$. Finally, because of the design of $\mathbf{P}_{\bar{\mathbf{R}}\mathcal{E}}$, the self response should be completely removed such that $\mathbf{R}\mathbf{P}_{\bar{\mathbf{R}}\mathcal{E}}^T \to \mathbf{0}$.

The dominating remaining term in this data block is the noise. This provides an area for the system's noise floor to be calculated. It is possible that this noise floor estimation can be corrupted by ϵ when a target is present. Various factors could cause the target response to leak into this data block. These errors could arise from factors such as: $\mathbf{P}_{\mathbf{R}}$ not being an accurate model (such as the edge effects of the filter), motion artifacts from the sensor, or sampling offset in real data since the measurements are not taken on an ideal equally-spaced grid of locations.

The average power of $\mathbf{M}_{\bar{\mathbf{G}}\mathbf{S}}^{\bar{\mathbf{R}}\mathcal{E}}$ from the WEMI lane data is shown in Fig. 11. Notice that strong targets often bleed over into this data block, especially when they are on the edge of the data matrix where $\mathbf{P}_{\mathbf{G}}$ does not isolate the target as well (as shown in 6d). Aside from the stronger targets, the noise floor remains fairly constant at roughly -135dB.

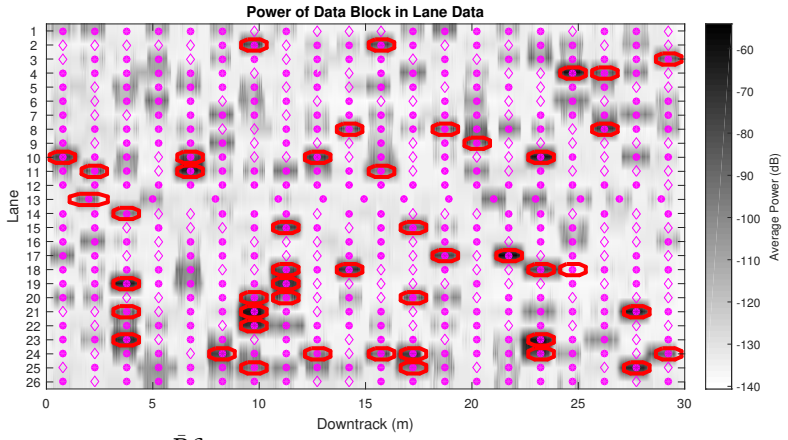

Figure 11: Average power of the $\mathbf{M}_{\mathbf{GS}}^{\bar{\mathbf{R}}\mathcal{E}}$ data block from measured WEMI data. This data block has the high spatial frequencies and is orthogonal from the soil subspace while aligning with the target's DSRF. This data is expected to be dominated by the noise, but strong targets can bleed into this data block due to positional error artifacts.

4.4 Investigating $\mathbf{M}_{\bar{\mathbf{G}}\mathcal{E}}^{\mathbf{RR}}$

The data block $\mathbf{M}_{\bar{\mathbf{G}}\mathcal{E}}^{\mathbf{RR}}$ is designed to contain the self response of the system when it overlaps with minimal distortion from the target and is orthogonal from the soil response. This is expressed mathematically as

$$\mathbf{P}_{\bar{\mathbf{G}}\mathcal{E}}\mathbf{M}\mathbf{P}_{\mathbf{RR}}^{T} = \cancel{\mathbf{P}_{\bar{\mathbf{G}}\mathcal{E}}\mathbf{S}\mathbf{P}_{\mathbf{RR}}^{T}}^{\epsilon\lambda_{\mathbf{G}\mathcal{E}}} + \cancel{\mathbf{P}_{\bar{\mathbf{G}}\mathcal{E}}\mathbf{G}\mathbf{P}_{\mathbf{RR}}^{T}}^{0} + \mathbf{P}_{\bar{\mathbf{G}}\mathcal{E}}\mathbf{R}\mathbf{P}_{\mathbf{RR}}^{T} + \mathbf{P}_{\bar{\mathbf{G}}\mathcal{E}}\mathcal{E}\mathbf{P}_{\mathbf{RR}}^{T} \tag{23}$$

where the target response and soil response are expected to be negligible in this data block. The soil response should be removed because $\mathbf{P}_{\bar{\mathbf{G}}\mathcal{E}}\mathbf{G} \rightarrow \mathbf{0}$. The target response is expected to be an extremely small value, $\epsilon\lambda_{\mathbf{G}\mathcal{E}}$. This is because the target will be removed for two reasons. First, the target will be removed from the spatial dimension as discussed previously such that $\mathbf{S}\mathbf{P}_{\mathbf{RR}}^{T} \rightarrow \epsilon$. Secondly, the target will be removed due to the measurement frequency projection. This is because $\mathbf{P}_{\bar{\mathbf{G}}\mathcal{E}}$ has been designed in such a way that $\mathbf{P}_{\bar{\mathbf{G}}\mathcal{E}}\mathbf{S} \rightarrow \lambda_{\mathbf{G}\mathcal{E}}$, where $\lambda_{\mathbf{G}\mathcal{E}}$ has been pre-selected as a small term. When both of these projections operate on $\mathbf{S}$, the resulting effect is that $\mathbf{P}_{\bar{\mathbf{G}}\mathcal{E}}\mathbf{S}\mathbf{P}_{\mathbf{RR}}^{T} \rightarrow \epsilon\lambda_{\mathbf{G}\mathcal{E}}$.

The self response of the system is the dominating term in this data block. It also has the minimal amount of corruption from other sources when compared to all the other data blocks. This creates the ideal data to calculate the strength of the system self response.

Fig. 12 shows the average power of this data block in the lane data, where the size is $\mathbf{M}_{\bar{\mathbf{G}}\mathcal{E}}^{\mathbf{RR}} \in \Re^{19\times 1}$. As can be seen, the average power does not correlate with targets except for the edges of strong targets when $\mathbf{P}_{\mathbf{G}}$ does not isolate it well. The data also shows that very little of the self response energy actually is contained in this data block. This is not too surprising as the self response can be modeled as the eddy currents induced in the platform and thus should also be decreased by $\mathbf{P}_{\bar{\mathbf{G}}\mathcal{E}}\mathbf{R} \rightarrow \lambda_{\mathbf{G}\mathcal{E}}$. Even though this means that the self response may not be estimated well here, it does serve as an ideal place to test the system calibration. This is because if the system is not calibrated well between measurement frequencies, then the DSRF model used for $\mathbf{P}_{\mathbf{G}}$ will no longer be valid and the self response will bleed into this data block. This provides evidence that the measured data was well calibrated since the average power is roughly -100 dB, which is $\lambda_{\mathbf{G}\mathcal{E}}$ lower than the 0 dB strength self response that will be seen in Fig. 15. This both provides an indicator for when the sensor's calibration is failing and potentially provides a method to adaptively calibrate the system.

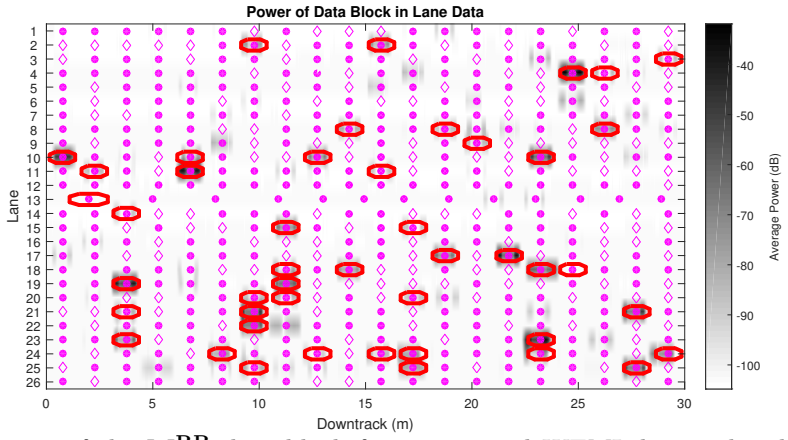

Figure 12: Average power of the $\mathbf{M}_{\bar{\mathbf{G}}\mathcal{E}}^{\mathbf{RR}}$ data block from measured WEMI data. This data block has the low spatial frequencies and is orthogonal from the soil subspace but does not align with the target's DSRF. This data is expected to be dominated by the self response.

4.5 Investigating $\mathbf{M}_{\bar{\mathbf{G}}\mathcal{E}}^{\bar{\mathbf{R}}\mathbf{S}}$

The data block $\mathbf{M}_{\bar{\mathbf{G}}\mathcal{E}}^{\bar{\mathbf{R}}\mathbf{S}}$ is designed to be isolated from both the self response and soil response and only have the minimal amount of target response. This is expressed mathematically as

$$\mathbf{P}_{\bar{\mathbf{G}}\mathcal{E}}\mathbf{M}\mathbf{P}_{\bar{\mathbf{R}}\mathbf{S}}^{T} = \cancel{\mathbf{P}_{\bar{\mathbf{G}}\mathcal{E}}\mathbf{S}\mathbf{P}_{\bar{\mathbf{R}}\mathbf{S}}^{T}}^{\lambda_{\mathbf{G}\mathcal{E}}} + \cancel{\mathbf{P}_{\bar{\mathbf{G}}\mathcal{E}}\mathbf{G}\mathbf{P}_{\bar{\mathbf{R}}\mathbf{S}}^{T}}^{0} + \cancel{\mathbf{P}_{\bar{\mathbf{G}}\mathcal{E}}\mathbf{R}\mathbf{P}_{\bar{\mathbf{R}}\mathbf{S}}^{T}}^{0} + \mathbf{P}_{\bar{\mathbf{G}}\mathcal{E}}\mathcal{E}\mathbf{P}_{\bar{\mathbf{R}}\mathbf{S}}^{T} \tag{24}$$

where the target response, soil response, and self response are expected to be negligible in this data block. Both the self response and soil response will be removed from the data block due to the design of the projection matrices such that $\mathbf{P}_{\bar{\mathbf{G}}\mathcal{E}}\mathbf{G} \to \mathbf{0}$ and $\mathbf{R}\mathbf{P}_{\bar{\mathbf{R}}\mathbf{S}}^{T} \to \mathbf{0}$. The target response is expected to be a small value that is roughly $\lambda_{\mathbf{G}\mathcal{E}}$ smaller than the target response. This is due to the cutoff threshold chosen when creating $\mathbf{P}_{\bar{\mathbf{G}}\mathcal{E}}$, where the target will be diminished by $\lambda_{\mathbf{G}\mathcal{E}}$.

This creates a data block that is most likely dominated by noise. This is another useful data block for estimating the noise power. The only factor other than noise is when strong targets are present in the measurements. If a target is $\lambda_{\mathbf{G}\mathcal{E}}$ stronger than the noise, then the target's energy will begin to bleed into this data block. Otherwise, the noise should dominate the target response and give accurate noise power estimations.

The lane data for the average power of $\mathbf{M}_{\bar{\mathbf{G}}\mathcal{E}}^{\bar{\mathbf{R}}\mathbf{S}}$ is shown in Fig. 13 where $\mathbf{M}_{\bar{\mathbf{G}}\mathcal{E}}^{\bar{\mathbf{R}}\mathbf{S}} \in \Re^{19\times 29}$ is the rough dimension depending on the number of spatial samples. As predicted, most of the measurements estimate a noise floor of roughly -130dB for the sensor. When a strong target is present, this estimate is distorted by the target bleeding into this data block, but this power is heavily reduced from the target's total power.

4.6 Investigating $\mathbf{M}_{\bar{\mathbf{G}}\mathcal{E}}^{\bar{\mathbf{R}}\mathcal{E}}$

The data block $\mathbf{M}_{\bar{\mathbf{G}}\mathcal{E}}^{\bar{\mathbf{R}}\mathcal{E}}$ is designed to solely contain noise that is orthogonal from the self response and soil response and the target response has minimal contribution. This is expressed mathematically as

$$\mathbf{P}_{\bar{\mathbf{G}}\mathcal{E}}\mathbf{M}\mathbf{P}_{\bar{\mathbf{R}}\mathcal{E}}^{T} = \cancel{\mathbf{P}_{\bar{\mathbf{G}}\mathcal{E}}\mathbf{S}\mathbf{P}_{\bar{\mathbf{R}}\mathcal{E}}^{T}}^{\epsilon\lambda_{\mathbf{G}\mathcal{E}}} + \cancel{\mathbf{P}_{\bar{\mathbf{G}}\mathcal{E}}\mathbf{G}\mathbf{P}_{\bar{\mathbf{R}}\mathcal{E}}^{T}}^{0} + \cancel{\mathbf{P}_{\bar{\mathbf{G}}\mathcal{E}}\mathbf{R}\mathbf{P}_{\bar{\mathbf{R}}\mathcal{E}}^{T}}^{0} + \mathbf{P}_{\bar{\mathbf{G}}\mathcal{E}}\mathcal{E}\mathbf{P}_{\bar{\mathbf{R}}\mathcal{E}}^{T} \tag{25}$$

where all sources but the noise term are negligible. The soil and self response are removed by their associated projection operators, $\mathbf{P}_{\bar{\mathbf{G}}\mathcal{E}}\mathbf{G} \to \mathbf{0}$ and $\mathbf{R}\mathbf{P}_{\bar{\mathbf{R}}\mathcal{E}}^{T} \to \mathbf{0}$. The target is expected to be an extremely small value that is $\epsilon\lambda_{\mathbf{G}\mathcal{E}}$ smaller than the total target energy. As discussed above, this is due to $\mathbf{P}_{\bar{\mathbf{G}}\mathcal{E}}$ causing the target to be reduced to $\mathbf{P}_{\bar{\mathbf{G}}\mathcal{E}}\mathbf{S} \to \lambda_{\mathbf{G}\mathcal{E}}$ and the $\mathbf{P}_{\bar{\mathbf{R}}\mathcal{E}}$ reducing the target to $\mathbf{S}\mathbf{P}_{\bar{\mathbf{R}}\mathcal{E}}^{T} \to \epsilon$.

This is the ideal data block to estimate the noise power. The data is isolated from both the soil and self response interferers. It also contains the least amount of target response out of all of the data blocks.

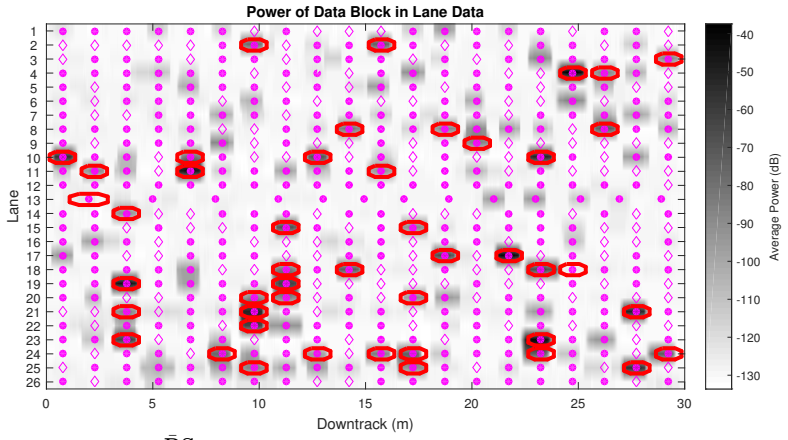

Figure 13: Average power of the $\mathbf{M}_{\bar{\mathbf{G}}\mathcal{E}}^{\bar{\mathbf{R}}\mathbf{S}}$ data block from measured WEMI data. This data block has the middle spatial frequencies and is orthogonal from the soil subspace but does not align with the target's DSRF. This data is expected to be dominated by noise, but can have strong target's bleed into it.

The average power of $\mathbf{M}_{\bar{\mathbf{G}}\mathcal{E}}^{\bar{\mathbf{R}}\mathcal{E}} \in \Re^{19\times 144}$ is shown in Fig. 14. This noise power estimate is more stable than any other data block (compare to Fig. 11 and 13). It shows that the noise floor of the WEMI system is close to -140dB. It has minimal power that bleeds in from strong targets. Even when targets do bleed in, the power is extremely reduced where it is less than -100dB except for the targets that overwhelm the sensor. It is also worth noting that this data block has roughly 2500 noise samples, so the estimated noise power is expected to be fairly reliable from this data block.

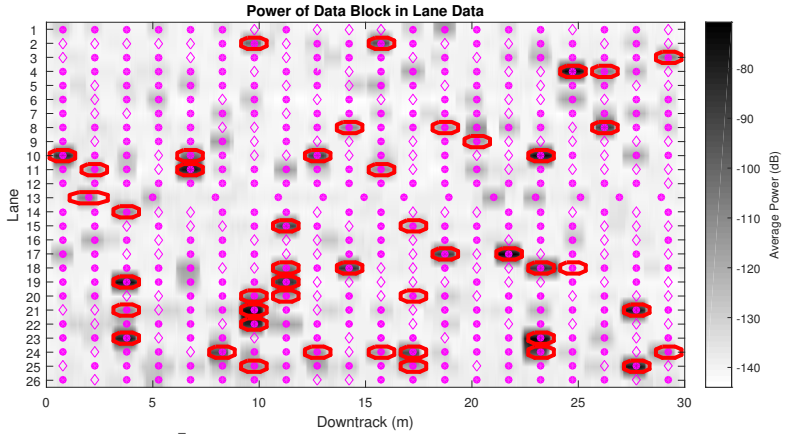

Figure 14: Average power of the $\mathbf{M}_{\bar{\mathbf{G}}\mathcal{E}}^{\bar{\mathbf{R}}\mathcal{E}}$ data block from measured WEMI data. This data block has the high spatial frequencies and is orthogonal from the soil subspace but does not align with the target's DSRF. This data is expected to be dominated by noise.

4.7 Investigating $\mathbf{M}_{\mathbf{GG}}^{\mathbf{RR}}$

The data block $\mathbf{M}_{\mathbf{GG}}^{\mathbf{RR}}$ is designed to contain the overlap of the soil response and self response in the measurements. This is expressed mathematically as

$$\mathbf{P}_{\mathbf{GG}}\mathbf{M}\mathbf{P}_{\mathbf{RR}}^{T} = \cancelto{\epsilon}{\mathbf{P}_{\mathbf{GG}}\mathbf{S}\mathbf{P}_{\mathbf{RR}}^{T}} + \mathbf{P}_{\mathbf{GG}}\mathbf{G}\mathbf{P}_{\mathbf{RR}}^{T} + \mathbf{P}_{\mathbf{GG}}\mathbf{R}\mathbf{P}_{\mathbf{RR}}^{T} + \mathbf{P}_{\mathbf{GG}}\mathcal{E}\mathbf{P}_{\mathbf{RR}}^{T}. \tag{26}$$

This data block is going to be heavily dominated by the interference components of the measurements. The self response, as mentioned before, can be orders of magnitude stronger than the target. As was seen in Fig. 1, a large portion of the self response overlaps with the soil response and thus is expected to reside in this data block.

Also, a large portion of the soil response resides here as well. Assuming the non-zero mean noise model of $\boldsymbol{\Xi}$, the constant term across positions will estimate the mean of both these distributions, g_1 and g_2, and place the energy in this data block. The combination of these interferences is expected to overwhelm the target when present. On the other hand, the quadrupole design of the receiver should cause $\mathbf{SP}_{\mathbf{RR}}^T \rightarrow \epsilon$ because the target should change signs as the quadrupole receiver passes over it. This means that very little target information is expected to be in this block. When solely interested in the target response, this block will have little value. However, if it is desired to extract information about either the soil response's average value or the strength of the self response then it can become useful.

Fig. 15 shows the average power for $\mathbf{M}_{\mathbf{GG}}^{\mathbf{RR}} \in \Re^{2\times 1}$ across all of the lanes. Comparing the average power of $\mathbf{M}_{\mathbf{GG}}^{\mathbf{RR}}$ to all other data blocks, it is clear that a majority of the measured power resides here. The power remains relatively stable at -25dB.

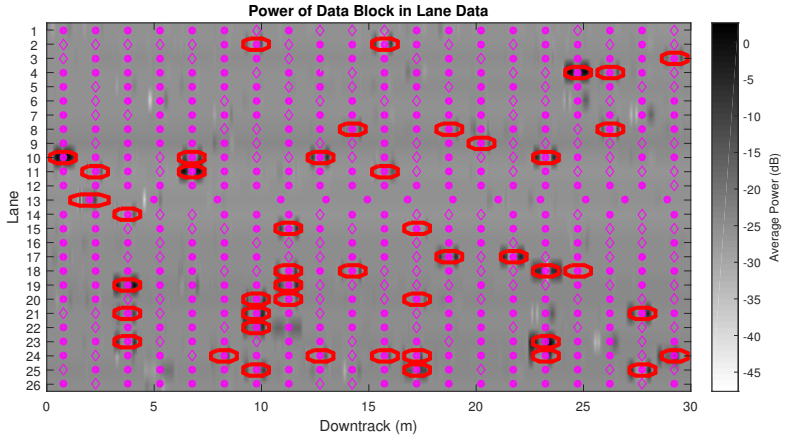

Figure 15: Average power of the $\mathbf{M}_{\mathbf{GG}}^{\mathbf{RR}}$ data block from measured WEMI data. This data block has the low spatial frequencies and contains the soil subspace. This data is expected to be dominated by the self response and soil response.

4.8 Investigating $\mathbf{M}_{\mathbf{GG}}^{\bar{\mathbf{R}}\mathbf{S}}$

The data block $\mathbf{M}_{\mathbf{GG}}^{\bar{\mathbf{R}}\mathbf{S}}$ is designed to contain the soil response that overlaps the target response but is orthogonal from the self response. This is expressed mathematically as

$$\mathbf{P}_{\mathbf{GG}}\mathbf{M}\mathbf{P}_{\bar{\mathbf{R}}\mathbf{S}}^T = \mathbf{P}_{\mathbf{GG}}\mathbf{S}\mathbf{P}_{\bar{\mathbf{R}}\mathbf{S}}^T + \mathbf{P}_{\mathbf{GG}}\mathbf{G}\mathbf{P}_{\bar{\mathbf{R}}\mathbf{S}}^T + \cancelto{0}{\mathbf{P}_{\mathbf{GG}}\mathbf{R}\mathbf{P}_{\bar{\mathbf{R}}\mathbf{S}}^T} + \mathbf{P}_{\mathbf{GG}}\mathcal{E}\mathbf{P}_{\bar{\mathbf{R}}\mathbf{S}}^T \tag{27}$$

where the self response of the system has been removed because $\mathbf{P}_{\bar{\mathbf{R}}\mathbf{S}}$ has been designed so $\mathbf{R}\mathbf{P}_{\bar{\mathbf{R}}\mathbf{S}}^T \rightarrow \mathbf{0}$. As was shown in Section 3.2, the target response overlaps the soil subspace through the projection $\mathbf{P}_{\mathbf{GG}}\mathbf{S}$. The position projection operator $\mathbf{P}_{\bar{\mathbf{R}}\mathbf{S}}$ is also designed to extract any variation that corresponds to an object below the transmitter. This means that $\mathbf{M}_{\mathbf{GG}}^{\bar{\mathbf{R}}\mathbf{S}}$ is expected to have a large amount of target information. Unfortunately this data is also strongly corrupted by the soil response. Depending on the permeability of the soil, the soil response can drastically reduce the amount of information that can be extracted from this data and can easily dominate many targets.

This data block is also potentially very interesting because it provides the opportunity to detect voids beneath the soil. This is because it concentrates the soil response into a small data block that also is extracting variations the size of the sensor. If a void exists beneath the ground, this would create an absence of the soil response. This absence would appear in the spatial domain very similar to a target response, and thus get highlighted in this data block. It is the author's belief that metrics from this data block could be used to detect such voids within the soil, especially in areas with a strong soil response.

The average power of $\mathbf{M}_{\mathbf{GG}}^{\bar{\mathbf{R}}\mathbf{S}} \in \Re^{2\times 29}$ is shown in Fig. 16. Many of the targets are still detectable in this data block, but the noise floor is noticeably higher than $\mathbf{M}_{\mathbf{GS}}^{\bar{\mathbf{R}}\mathbf{S}}$. The noise and interference floor has been increased to roughly -80dB for this data block due to the soil response. The increase in the noise and interference floor of around 50dB compared to $\mathbf{M}_{\mathbf{GS}}^{\bar{\mathbf{R}}\mathbf{S}}$ illustrates that the target power of roughly 7.1dB that is lost when using $\mathbf{P_G}$ to isolate the target from the soil response is recouped from the interference isolation. However, it is still desirable to extract the target power contained in this data block as well.

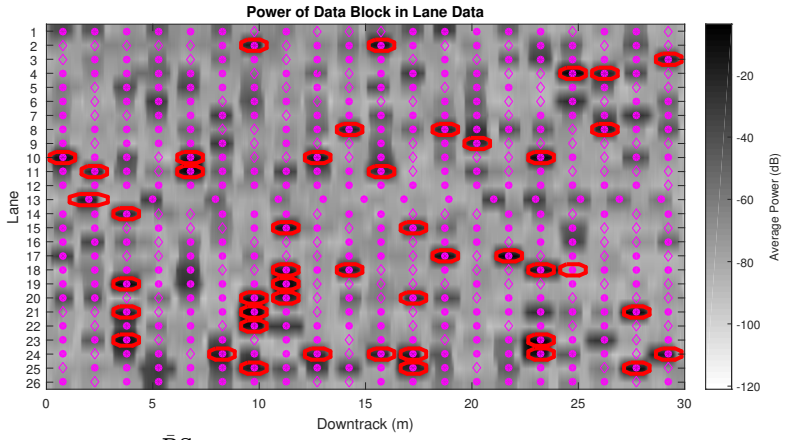

Figure 16: Average power of the $\mathbf{M}_{\mathbf{GG}}^{\bar{\mathbf{R}}\mathbf{S}}$ data block from measured WEMI data. This data block has the middle spatial frequencies and contains the soil subspace. This data is expected to be a mixture of the target response and soil response.

In order to exploit the target data in $\mathbf{M}_{\mathbf{GG}}^{\bar{\mathbf{R}}\mathbf{S}}$, it is ideal to further isolate it from the soil response. From the SVD of $\mathbf{M}_{\mathbf{GS}}^{\bar{\mathbf{R}}\mathbf{S}}$, the spatial response of the target is contained in $\mathbf{V}_{\mathbf{S}}^{\mathbf{M_S}}$. As long as the target is strong enough in $\mathbf{M}_{\mathbf{GS}}^{\bar{\mathbf{R}}\mathbf{S}}$ to be isolated in the strongest three singular values, then the spatial response of the target is described by ${\mathbf{V}_{\mathbf{S}}^{\mathbf{M_S}}}^T\mathbf{P}_{\bar{\mathbf{R}}\mathbf{S}}$. Using this knowledge, it is possible to isolate the data in $\mathbf{M}_{\mathbf{GG}}^{\bar{\mathbf{R}}\mathbf{S}}$ that corresponds to the target's spatial response by creating an adaptive matched subspace filter bank. This is accomplished by creating the spatial signal projection matrix $\mathbf{P_S} = \mathbf{V}_{\mathbf{S}}^{\mathbf{M_S}}({\mathbf{V}_{\mathbf{S}}^{\mathbf{M_S}}}^T\mathbf{V}_{\mathbf{S}}^{\mathbf{M_S}})^{-1}{\mathbf{V}_{\mathbf{S}}^{\mathbf{M_S}}}^T$. The data block can then be separated into two sub-blocks

$$\mathbf{M}_{\mathbf{GG}}^{\bar{\mathbf{R}}\mathbf{S}} = \mathbf{M}_{\mathbf{GG}}^{\bar{\mathbf{R}}\mathbf{S}}\mathbf{P}_{\mathbf{S}}^T + \mathbf{M}_{\mathbf{GG}}^{\bar{\mathbf{R}}\mathbf{S}}{\mathbf{P}_{\mathbf{S}}^{\perp}}^T \tag{28}$$

where $\mathbf{P}_{\mathbf{S}}^{\perp} = \mathbf{I} - \mathbf{P_S}$ is the projection operator orthogonal to $\mathbf{P_S}$. The target response should be contained in $\mathbf{M}_{\mathbf{GG}}^{\bar{\mathbf{R}}\mathbf{S}}\mathbf{P}_{\mathbf{S}}^T$ and the soil response power will be decreased by a factor of $\frac{3}{P}$ under the Gaussian soil assumption. The remaining sub-block $\mathbf{M}_{\mathbf{GG}}^{\bar{\mathbf{R}}\mathbf{S}}{\mathbf{P}_{\mathbf{S}}^{\perp}}^T$ should have minimal target response and be dominated by the soil response.

The average power of the target and noise sub-blocks of $\mathbf{M}_{\mathbf{GG}}^{\bar{\mathbf{R}}\mathbf{S}}$ are shown in Fig. 17 and 18 respectively. It can be seen that the power of a target remains mostly unchanged in $\mathbf{M}_{\mathbf{GG}}^{\bar{\mathbf{R}}\mathbf{S}}\mathbf{P}_{\mathbf{S}}^T$ compared to $\mathbf{M}_{\mathbf{GG}}^{\bar{\mathbf{R}}\mathbf{S}}$ and the interference floor is slightly reduced. It is also compelling that Fig. 18 is fairly constant and minimally correlates to the presence of a target. This shows that the target response has been further isolated from the soil response. This process also provides a data sub-block that can be used to obtain an accurate estimate of the noise and interference floor.

4.9 Investigating $\mathbf{M}_{\mathbf{GG}}^{\bar{\mathbf{R}}\mathcal{E}}$

The data block $\mathbf{M}_{\mathbf{GG}}^{\bar{\mathbf{R}}\mathcal{E}}$ is designed to contain the soil response that is orthogonal to the self response and contains minimal target energy. This is expressed mathematically as

$$\mathbf{P_{GG}}\mathbf{M}\mathbf{P}_{\bar{\mathbf{R}}\mathcal{E}}^T = \cancelto{\epsilon}{\mathbf{P_{GG}}\mathbf{S}\mathbf{P}_{\bar{\mathbf{R}}\mathcal{E}}^T} + \mathbf{P_{GG}}\mathbf{G}\mathbf{P}_{\bar{\mathbf{R}}\mathcal{E}}^T + \cancelto{0}{\mathbf{P_{GG}}\mathbf{R}\mathbf{P}_{\bar{\mathbf{R}}\mathcal{E}}^T} + \mathbf{P_{GG}}\mathcal{E}\mathbf{P}_{\bar{\mathbf{R}}\mathcal{E}}^T \tag{29}$$

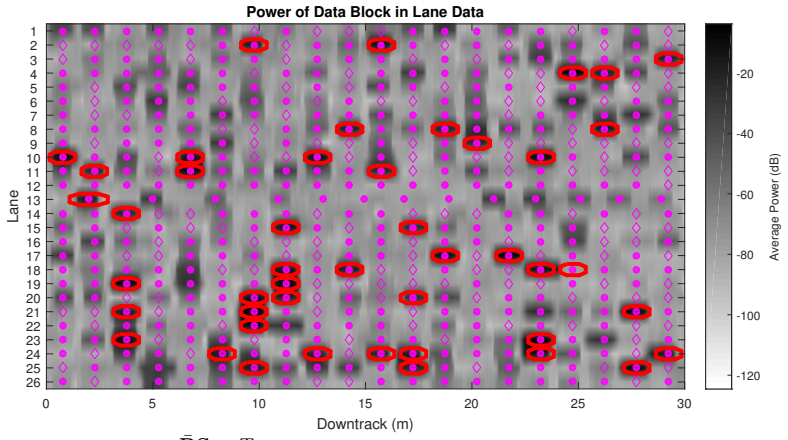

Figure 17: Average power of the $\mathbf{M}_{\mathbf{GG}}^{\bar{\mathbf{R}}\mathbf{S}}\mathbf{P}_{\mathbf{S}}^{T}$ data block from measured WEMI data. This data block has the power in $\mathbf{M}_{\mathbf{GG}}^{\bar{\mathbf{R}}\mathbf{S}}$ that aligns with the measured spatial response of the target. This data is expected to contain the self response where the soil response has been reduced.

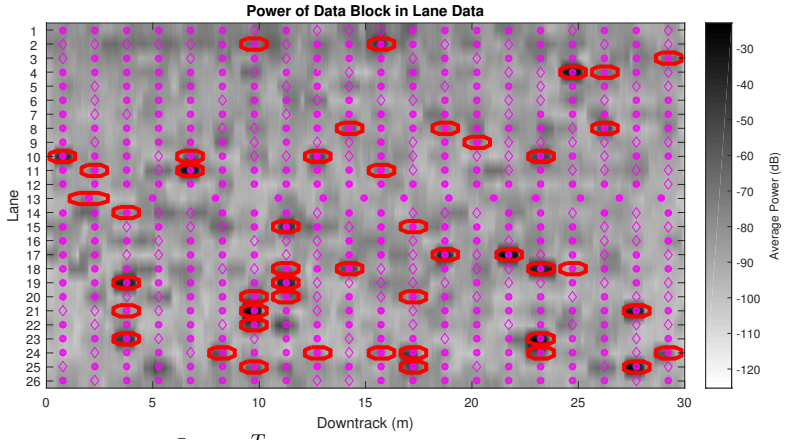

Figure 18: Average power of the $\mathbf{M}_{\mathbf{GG}}^{\bar{\mathbf{R}}\mathbf{S}}\mathbf{P}_{\mathbf{S}}^{\perp\,T}$ data block from measured WEMI data. This data block has the power in $\mathbf{M}_{\mathbf{GG}}^{\bar{\mathbf{R}}\mathbf{S}}$ that does not align with the measured spatial response of the target. This data is expected to be dominated by the soil response.

where there is minimal impact from the target response and self response. The self response is again removed because $\mathbf{R}\mathbf{P}_{\bar{\mathbf{R}}\mathcal{E}}^{T} \rightarrow \mathbf{0}$. The target response is diminished to some small number due to the position projection matrix because $\mathbf{S}\mathbf{P}_{\bar{\mathbf{R}}\mathcal{E}}^{T} \rightarrow \epsilon$.

This creates an ideal data block for estimating the variance of the soil response. Because the mean of the soil response has been removed (since it is contained in $\mathbf{M}_{\mathbf{GG}}^{\mathbf{RR}}$), the strongest component in this data block is expected to be the soil's variation. The data block also contains the noise component, but it is expected that the soil response is stronger than the system noise level and will thus dominate these measurements. Alternatively, the combination of the soil response and noise response can be thought of as an interference level in the data block $\mathbf{M}_{\mathbf{GG}}^{\bar{\mathbf{R}}\mathbf{S}}$. This allows the interference floor to be estimated to further enable processing on $\mathbf{M}_{\mathbf{GG}}^{\bar{\mathbf{R}}\mathbf{S}}$. Also, this provides ideal data for testing how strong the soil response is in a specific area, regardless of the presence or absence of a target. If the interference level in this data block is compared to a noise data block, such as $\mathbf{M}_{\mathbf{G}\mathcal{E}}^{\bar{\mathbf{R}}\mathcal{E}}$, then it is possible to estimate how much stronger the soil response variation is from the noise variation. This information could be used to determine if it is better to project the target data away from the soil interference for processing and take the target response decrease $\lambda_{\mathbf{G}\mathcal{E}}$, or if the soil response is weak enough that $\mathbf{M}_{\mathbf{GS}}^{\bar{\mathbf{R}}\mathbf{S}}$ and $\mathbf{M}_{\mathbf{GG}}^{\bar{\mathbf{R}}\mathbf{S}}$ should be processed together. Estimating the interference level can also allow for the measurements in $\mathbf{M}_{\mathbf{GS}}^{\bar{\mathbf{R}}\mathbf{S}}$ and $\mathbf{M}_{\mathbf{GG}}^{\bar{\mathbf{R}}\mathbf{S}}$ to be properly whitened so processing can correctly extract information from $\mathbf{M}_{\mathbf{GS}}^{\bar{\mathbf{R}}\mathbf{S}}$ and $\mathbf{M}_{\mathbf{GG}}^{\bar{\mathbf{R}}\mathbf{S}}$

jointly from any data regardless of the soil response's strength.

Fig. 19 shows the average power of $\mathbf{M}_{\mathbf{GG}}^{\bar{\mathbf{R}}\mathcal{E}} \in \Re^{2\times 144}$ through the lanes. Strong targets bleed into this data block due to $\mathbf{P_R}$. Otherwise, this data block is fairly consistent and provides an opportunity to estimate the interference plus noise level.

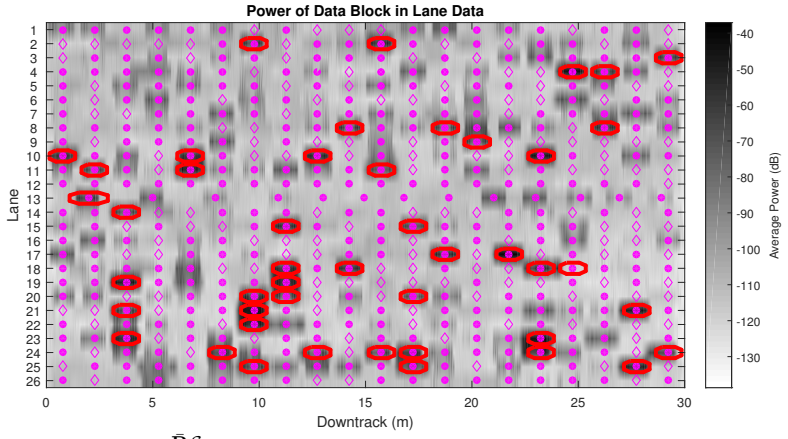

Figure 19: Average power of the $\mathbf{M}_{\mathbf{GG}}^{\bar{\mathbf{R}}\mathcal{E}}$ data block from measured WEMI data. This data block has the high spatial frequencies and contains the soil subspace. This data is expected to be dominated by the soil response.

5. CONCLUSION

This work has provided an in-depth analysis of the filterless pre-processing for frequency-domain WEMI sensors. The filterless pre-processing operates by defining the projection matrices $\mathbf{P_G}$ and $\mathbf{P_R}$ to isolate the interference signals in the measured data matrix. A detailed description of how to create $\mathbf{P_G}$ and $\mathbf{P_R}$ were both provided. The design for $\mathbf{P_R}$ was based on using a quadrupole receiver for the WEMI system, where the projection operator parameters are based on the dimensions of the receiver. When designing $\mathbf{P_G}$, a maximum desired SNR for any target response must be selected. It was shown in Fig. 3 that this selection can be limited if the WEMI system does not provide enough measurement frequencies to reach the desired SNR cutoff. It was also shown in Fig. 4 that a large amount of the target response will be contained in the soil subspace.

Using the described filterless pre-processing scheme, the measured data matrix is portioned into nine data blocks as shown in Fig. 2. This work provided a mathematical description of the expected data within each of these data blocks. Data was processed from the Georgia Tech WEMI system to produce each of the nine data blocks, and the resulting average power was shown to corroborate with the mathematical model. Two data blocks are expected to have a large amount of energy from the target response: $\mathbf{M}_{\mathbf{GS}}^{\bar{\mathbf{R}}\mathbf{S}}$ and $\mathbf{M}_{\mathbf{GG}}^{\bar{\mathbf{R}}\mathbf{S}}$. Analysis was performed on $\mathbf{M}_{\mathbf{GS}}^{\bar{\mathbf{R}}\mathbf{S}}$ to show that a SVD can further isolate the target response and the improved measurements are shown in Fig. 9. The expected SNR improvement from the SVD calculation is provided in (21). It was also shown that $\mathbf{M}_{\mathbf{GG}}^{\bar{\mathbf{R}}\mathbf{S}}$ can be adaptively processed based on the SVD of $\mathbf{M}_{\mathbf{GS}}^{\bar{\mathbf{R}}\mathbf{S}}$ to improve the SINR of the target response in $\mathbf{M}_{\mathbf{GG}}^{\bar{\mathbf{R}}\mathbf{S}}$. The results were shown in Fig. 17. This work discussed the potential to exploit these data blocks to provide accurate noise power estimations, void detection, and adaptive calibration capabilities.

ACKNOWLEDGMENTS

This work is supported in part by the U.S. Army REDCOM CERDEC Night Vision and Electronic Sensors Directorate, Science and Technology Division, Countermine Branch and in part by the U. S. Army Research Office under Contract Number W911NF-11-1-0153.

REFERENCES

[1] Hayes, C. E., McClellan, J. H., and Scott Jr., W. R., "Novel model based EMI processing framework," in [*Detection and Sensing of Mines, Explosive Objects, and Obscured Targets XXII*], **10182**, 1018218, International Society for Optics and Photonics (2017).

[2] Hayes, C. E., Scott Jr., W. R., and McClellan, J. H., "Low-rank model for wideband electromagnetic induction sensors," *IEEE Geoscience and Remote Sensing Letters* **14**(12), 2413–2417 (2017).

[3] Bruschini, C., *A Multidisciplinary Analysis of Frequency Domain Metal Detectors for Humanitarian Demining*, PhD thesis, Vrije Universiteit Brussel (September 2002).

[4] Wei, M.-H., Scott Jr., W. R., and McClellan, J. H., "Adaptive prefiltering for nonnegative discrete spectrum of relaxations," *Geoscience and Remote Sensing Letters, IEEE* **12**, 1018–1022 (May 2015).

[5] Hayes, C. E., McClellan, J. H., Scott Jr., W. R., and Kerr, A. J., "Improved electromagnetic induction processing with novel adaptive matched filter and matched subspace detection," *Proc. SPIE* **9823**, 98230E–98230E–14 (2016).

[6] Krueger, K., Scott Jr., W. R., and McClellan, J. H., "Location and orientation estimation of buried targets using electromagnetic induction sensors," *Proc. SPIE* **8357**, 8357 – 8357 – 12 (2012).

[7] Scott Jr., W. R., Larson, G. D., Hayes, C. E., and McClellan, J. H., "Experimental detection and discrimination of buried targets using an improved broadband CW electromagnetic induction sensor," *Proc. SPIE* **9072**, 90720C–90720C–15 (2014).

[8] Hayes, C. E., McClellan, J. H., and Scott Jr., W. R., "Sparse recovery using an SVD approach to interference removal and parameter estimation," *IEEE Signal Processing & SP Education Workshop* , 202–207 (2015).

[9] Wei, M. H., Scott Jr., W. R., and McClellan, J. H., "Robust estimation of the discrete spectrum of relaxations for electromagnetic induction responses," *IEEE Transactions on Geoscience and Remote Sensing* **48**, 1169–1179 (March 2010).